JOURNAL OF THERMOPHYSICS AND HEAT TRANSFER
Vol. 7, No. 3, July–Sept. 1993

Laminar Free Convection in a Nonrectangular Inclined Cavity

George N. Facas*
Trenton State College, Trenton, New Jersey 08650

Numerical calculations are presented for two-dimensional natural convection flow in a nonrectangular inclined cavity. The governing equations in the stream function-vorticity formulation are solved using finite differences. Arakawa's differencing scheme is used to represent the convection terms. Flow characteristics are investigated for Grashof numbers and inclination angles in the range of 9.0×10^3 to 1.25×10^5, and -30 to 30 deg (from the vertical), respectively. A multicellular flow structure is found to exist for all angles of inclination considered. Although steady-state solutions were achieved for all Grashof numbers and angles of inclination considered, the flow structure that was predicted (steady vs unsteady) was found to depend strongly on the initial condition and, in some cases, unsteady flows were predicted if the "wrong" initial condition was specified.

Nomenclature

a = cavity width
d = cavity length
Gr = Grashof number, $g\beta\Delta Ta^3/\nu^2$
Pr = Prandtl number, ν/α
T = temperature
u' = nondimensional velocity
u, v = velocity component in x and y direction
v' = nondimensional velocity
α = thermal diffusivity
β = volumetric expansion coefficient
ζ = nondimensional spatial coordinate
Θ = nondimensional temperature
ϑ = inclination angle
λ = cavity aspect ratio, d/a
ν = kinematic viscosity
ξ = nondimensional spatial coordinate
ρ = density
τ = nondimensional time
Ψ = nondimensional stream function
ψ = stream function
Ω = nondimensional vorticity
ω = vorticity

Introduction

NATURAL convection in long enclosures has received much attention because of its many engineering applications which include double-pane windows, solar collectors, double-wall insulation, and nuclear reactor insulation. Two excellent comprehensive review articles on the subject have been written by Catton[1] and Ostrach.[2]

It is generally known that for a cavity heated on one side and cooled on the opposite side, the fluid flow is characterized by a single large cell; the fluid ascends along the hot wall, descends along the cold wall, and turns at the opposite ends of the cavity. For small Grashof numbers, the flow is weak and the isotherms are parallel to the vertical walls. In this region, heat is transferred by conduction across the fluid. This flow regime was first analyzed by Batchelor,[3] who named it the conduction regime. With increasing Grashof number, however, this flow becomes unstable. Hart[4] and Korpela et al.[5] showed that the instability takes different forms depending on the fluid Prandtl number. In the limit of zero Prandtl number, the instability is purely hydrodynamic and leads to transverse cells. For large Prandtl numbers, the instability takes the form of traveling waves. Experiments performed by Elder,[6] using water to visualize the boundary layers along the vertical walls, have shown the presence of secondary stationary motions in the interior of the cavity. These findings have been confirmed by many other experimental and numerical studies.[7–14]

Roux et al.[15] showed that these secondary motions can only be observed in air-filled cavities of aspect ratio greater than a critical value between 11 and 12. Roux et al. have also shown that as the Grashof number further increases, the flow structure changes from multicellular to monocellular and it becomes one of a boundary-layer type. The analytical work of Gill[16] has further shown that the flowfield structure in the core region of the cavity is vertically stratified, which is consistent with the experimental observations by Elder.[6] However, it is not clear at this time whether this reverse transition from multicellular to unicellular flow actually occurs. The experimental studies performed by Pignatel and Marcillat[13] indicated a return to steady unicellular flow. However, Lauriat and Desrayaud[12] never saw such a return to unicellular flow and reported a chaotic motion.

Hart[4] was the first to carry experiments with an inclined rectangular cavity of large aspect ratio using water. Linthorst et al.[11] performed experiments with air-filled inclined rectangular cavities of small and moderate aspect ratio, and angles of inclination from 0 to negative 90 deg, which represents only heating from below. Their results show that at moderate angles of inclination from the vertical, the instability is still hydrodynamic and it takes the form of transverse cells; however, at large angles of inclination, the stability is buoyancy driven and it takes the form of longitudinal rolls with the cell axes aligned along the cavity length.

Ozoe et al.[17] performed experiments with air-filled rectangular cavities of aspect ratio in the range of 8.4–15.5 and inclination angles from 0 to 180 degrees (relative to the horizontal). However, at low inclination angles relative to the vertical, they presented heat transfer results only for Rayleigh numbers below 3760. Unicellular flow was observed at low inclination angles relative to the vertical for the low range of Rayleigh numbers investigated.

More recently, Pignatel and Marcillat[13] carried experiments with air-filled inclined rectangular cavities of aspect ratio in the range of 10–17, and angles of inclination from 0 to negative 90 deg (all cases represent heating from below). Their results for cavities of large aspect ratio show that at moderate angles of inclination from the vertical (less than 30 deg from the vertical) the flow can be assumed to be two-dimensional.

Presented as Paper 92-0714 at the AIAA 30th Aerospace Sciences Meeting and Exhibit, Reno, NV, Jan. 6–9, 1992; received Jan. 17, 1992; revision received Aug. 3, 1992; accepted for publication Aug. 3, 1992.

*Assistant Professor, Mechanical Engineering. Member AIAA.

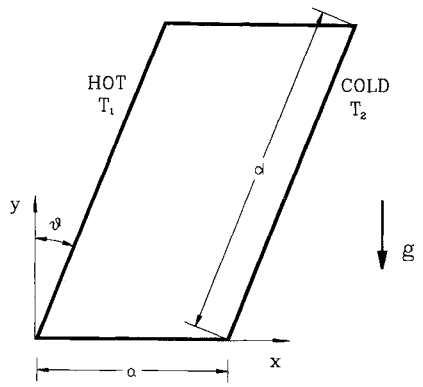

Fig. 1 Geometry and configuration.

Moreover, their results show that steady as well as unsteady flow structures are found, depending on the value of the Grashof number. Their results also show that the reverse transition occurs for cavity aspect ratios greater than 11 and $\vartheta > \vartheta_{cr}$, where the critical angle is a function of the cavity aspect ratio.

In the present study, flow characteristics are investigated numerically for an air-filled inclined, nonrectangular cavity as shown in Fig. 1. The left inclined wall of the cavity is assumed to be maintained at a constant temperature T_1, whereas, the right wall is maintained at a constant temperature T_2, with $T_1 > T_2$. Both the top and bottom horizontal surfaces are assumed to be adiabatic. The present study was restricted to cavities with aspect ratio of 15 and a fluid Prandtl number of 0.71. Results have been obtained for Grashof numbers ranging from 9.0×10^3 to 1.25×10^5, and angles of inclination from -30 to 30 deg. Note that a negative value for the inclination angle is argued to represent heating from below, whereas, a positive value is assumed to represent heating from above.

Mathematical Formulation

Consider the two-dimensional nonrectangular inclined cavity of a and d which contains a Newtonian fluid, as shown schematically in Fig. 1. The problem is to find the velocity and temperature profile inside the cavity, as well as the rate of heat transfer across the inclined walls of the cavity, assuming that one of the inclined walls is heated to a constant temperature T_1 while the other is cooled to a constant temperature T_2.

For natural convection flows with small density changes, it is common to employ the Boussinesq approximation,[18] i.e., to assume that the effect of temperature on density is confined only to the body force term of the momentum equation and that all other fluid properties are independent of temperature and pressure. This implies that the fluid is incompressible, and its equation of state is

$$\rho = \rho_0[1 - \beta(T - T_0)] \tag{1}$$

where ρ and β represent the density and the volumetric expansion coefficient, respectively, and the subscript denotes some reference state.

Using the stream function-vorticity approach, the governing equations with the Boussinesq approximation for two-dimensional laminar-free convection are

Stream function equation

$$\frac{\partial^2\psi}{\partial x^2} + \frac{\partial^2\psi}{\partial y^2} = -\omega \tag{2}$$

Vorticity transport equation

$$\frac{\partial\omega}{\partial t} + u\frac{\partial\omega}{\partial x} + v\frac{\partial\omega}{\partial y} = v\left(\frac{\partial^2\omega}{\partial x^2} + \frac{\partial^2\omega}{\partial y^2}\right) + g\rho\beta\frac{\partial T}{\partial x} \tag{3}$$

Energy equation

$$\frac{\partial T}{\partial t} + u\frac{\partial T}{\partial x} + v\frac{\partial T}{\partial y} = \alpha\left(\frac{\partial^2 T}{\partial x^2} + \frac{\partial^2 T}{\partial y^2}\right) \tag{4}$$

where

$$u = \frac{\partial\psi}{\partial y} \qquad v = -\frac{\partial\Psi}{\partial x} \tag{5}$$

$$\omega = \frac{\partial v}{\partial x} - \frac{\partial u}{\partial y} \tag{6}$$

In general, no rectangular grid mesh can be generated that fits all four surfaces. However, the computational domain can be mapped onto a rectangular domain by using the transformations:

$$x' = x - y\tan\vartheta \qquad -90 \text{ deg} < \vartheta < 90 \text{ deg}$$
$$y' = y \tag{7}$$

With this transformation and in dimensionless form, the governing Eqs. (2–4) become

$$\frac{\partial^2\Psi}{\partial\xi^2} - 2\frac{\sin\vartheta}{\lambda}\frac{\partial^2\Psi}{\partial\xi\partial\zeta} + \frac{1}{\lambda^2}\frac{\partial^2\Psi}{\partial\zeta^2} = -\cos^2\vartheta\Omega \tag{8}$$

$$\cos\vartheta\frac{\partial\Omega}{\partial\tau} + u'\frac{\partial\Omega}{\partial\xi} + v'\frac{\partial\Omega}{\partial\zeta} = \frac{1}{\cos\vartheta}\left(\frac{\partial^2\Omega}{\partial\xi^2} - 2\frac{\sin\vartheta}{\lambda}\cdot\frac{\partial^2\Omega}{\partial\xi\partial\zeta} + \frac{1}{\lambda^2}\frac{\partial^2\Omega}{\partial\zeta^2}\right) + Gr\cos\vartheta\frac{\partial\Theta}{\partial\xi} \tag{9}$$

$$\cos\vartheta\frac{\partial\Theta}{\partial\tau} + u'\frac{\partial\Theta}{\partial\xi} + v'\frac{\partial\Theta}{\partial\zeta} = \frac{1}{Pr\cos\vartheta}\left(\frac{\partial^2\Theta}{\partial\xi^2} - 2\frac{\sin\vartheta}{\lambda}\frac{\partial^2\Theta}{\partial\xi\partial\zeta} + \frac{1}{\lambda^2}\frac{\partial^2\Theta}{\partial\zeta^2}\right) \tag{10}$$

where

$$Gr = [g\beta(T_1 - T_2)a^3/\nu^2], \quad \lambda = (d/a), \quad Pr = (\nu/\alpha)$$
$$x' = a\xi, \quad y' = (d\cos\vartheta)\zeta, \quad \psi = \nu\Psi, \quad \omega = (\nu/a^2)\Omega$$
$$t = (a^2/\nu)\tau, \quad \Theta = [(T - T_2)/(T_1 - T_2)]$$

Note that

$$u' = \frac{1}{\lambda}\frac{\partial\Psi}{\partial\zeta}$$
$$v' = -\frac{1}{\lambda}\frac{\partial\Psi}{\partial\xi} \tag{11}$$

In the dimensionless coordinates, the computational domain extends in both directions from 0 to 1. The solution to Eqs. (8–10) with the appropriate boundary conditions, yields the desired distribution for Ψ, Ω, and Θ.

Boundary Conditions

The no-slip condition at the walls, $u = v = 0$, yields $\Psi =$ const. Thus, at the two inclined walls and the bottom and top wall, the value $\Psi = 0$ is arbitrarily assigned.

With regards to vorticity, a new approach has been used to evaluate the vorticity near the boundaries, as outlined by Baron.[19] Facas and Mattioli[20] showed that computational savings can result when this method is used to evaluate the vorticity near solid walls. In this new approach, it is not necessary

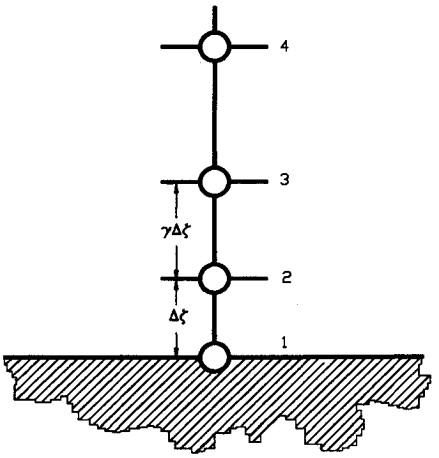

Fig. 2 Grid points near the wall.

to specify conditions for the vorticity at the boundaries. Instead, the vorticity is calculated using the no-slip condition at the wall (without fluid injection or fluid suction, one requires that $\partial\Psi/\partial n = 0$, where n is in the direction normal to the wall) and the stream function equation. For the grid shown in Fig. 2, one can write the following second-order accurate finite difference expression at the wall:

$$\frac{\partial\Psi}{\partial\zeta} = \frac{1}{\gamma(\gamma+1)\Delta\zeta}[-\gamma(\gamma+2)\Psi_1 + (1+\gamma)^2\Psi_2 - \Psi_3] \tag{12}$$

In the method outlined by Baron, the computational procedure is as follows: the stream function-vorticity equations are solved in the regular manner all the way down to point 3 (note that in order to solve for Ψ and Ω at point 3, values for Ψ and Ω are required at point 2 but not at point 1). Since the no-slip condition requires that $\partial\Psi/\partial\zeta = 0$ at the solid wall (point 1) and Ψ_1 and Ψ_3 are both known (Ψ_1 is specified, Ψ_3 is calculated from last iteration), the value for Ψ_2 is calculated using Eq. (12). Once the new value for Ψ_2 is obtained, Ω_2 is calculated by simply substituting the required Ψ_{ij} values in Eq. (8).

As outlined in this method, the no-slip condition was imposed on all four walls. Thus

$$\frac{\partial\Psi}{\partial\xi} = 0 \quad \xi = 0, 1 \qquad \frac{\partial\Psi}{\partial\zeta} = 0 \quad \zeta = 0, 1 \tag{13}$$

Constant uniform temperatures T_1 and T_2 ($T_1 > T_2$) are imposed at the left and right inclined walls, respectively. The top and bottom walls are assumed to be adiabatic. Thus

$$\Theta = 1 \quad \xi = 0, \qquad \Theta = 0 \quad \xi = 1$$

$$\frac{\partial\Theta}{\partial\zeta} - \lambda \sin\vartheta \frac{\partial\Theta}{\partial\xi} = 0 \quad \zeta = 0, 1 \tag{14}$$

Method of Solution

The system of equations with the boundary conditions is solved using finite differences. The Arakawa's differencing scheme[21] is used with the convective terms, and central differences are used with the diffusive terms. The Arakawa's scheme was selected for this problem because it has been demonstrated[8,9] that it can predict the transition to multicellular flow which exists in this problem. First-order accurate forward differences were used with the time derivative.

The majority of the calculations were made using both a 31 × 91 as well as a 51 × 151 uniform grid mesh. A dimensionless time step of 5×10^{-4} was used with the finer grid mesh, and 1×10^{-3} with the coarser grid. The solution to the algebraic system of equations at the end of each time step has been obtained using the modified strongly implicit procedure method.[22] The steady-state solution was assumed to have been reached when the residual between time steps was less than 10^{-4} for all three variables at every grid point. Typically, when this criterion was met, the average residual between time steps for the temperature field was in the order of 10^{-9}, whereas, the average residuals for the stream function and vorticity fields were in the order of 10^{-6} and 10^{-5}, respectively. All computations were carried out on a 386 personal computer.

Results and Discussion

In view of the large number of parameters involved in this problem, the present study was restricted to cavities with aspect ratios of 15, and a fluid Prandtl number of 0.71. Numerical calculations were performed for values of Grashof number up to 1.25×10^5 and inclination angles in the range −30 to 30 deg from the vertical.

The effects of inclination on the structure of the flow are illustrated in Figs. 3 and 4 for an inclination angle of negative 30 deg. As shown in Fig. 3, the flow is clearly monocellular for a Grashof number up to 1.2×10^4, and it exhibits the characteristics of the conduction regime. However, as Gr in-

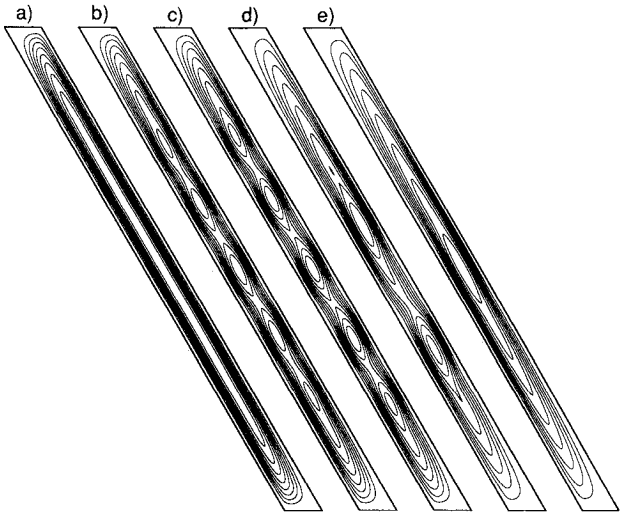

Fig. 3 Stream function contours for $\vartheta = -30$ deg: a) $Gr = 1.2 \times 10^4$, b) $Gr = 1.5 \times 10^4$, c) $Gr = 2.0 \times 10^4$, d) $Gr = 6.0 \times 10^4$, e) $Gr = 8.0 \times 10^4$.

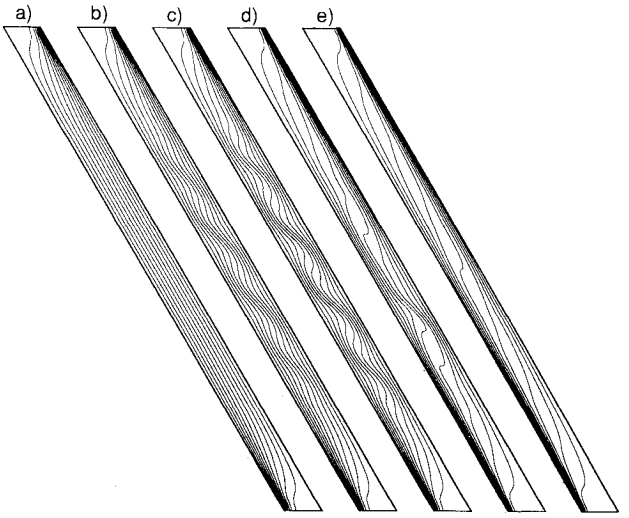

Fig. 4 Isotherms for $\vartheta = -30$ deg: a) $Gr = 1.2 \times 10^4$, b) $Gr = 1.5 \times 10^4$, c) $Gr = 2.0 \times 10^4$, d) $Gr = 6.0 \times 10^4$, e) $Gr = 8.0 \times 10^4$.

creases to 1.5×10^4, the flow is characterized by three central cells and two weaker outer cells. As Gr further increases to a value of 2.0×10^4, the two outer cells grow to the same intensity as the central three cells. The solutions shown in Figs. 3 and 4 for Gr values up to 2.0×10^4 are steady-state solutions. The steady-state solutions corresponding to Gr values of 1.2×10^4 and 1.5×10^4 were achieved at a dimensionless time approximately equal to 3, whereas, the steady-state solution corresponding to $Gr = 2.0 \times 10^4$ was obtained after a long integration to a dimensionless time approximately equal to 15.0.

Starting from the steady solution corresponding to $Gr = 2.0 \times 10^4$ as the initial condition, and increasing the Gr value to 6.0×10^4, a three-cell unsteady flow structure is predicted by this numerical scheme for both grid meshes considered. The time trace of the temperature (Fig. 5) at a point located along the vertical centerline and at $\zeta = 0.43$, indicates time-periodic fluctuations of constant amplitude when a grid mesh of 51×151 and a time step of 5×10^{-4} was used. In order to ensure that these findings are independent of the time step used, the computations were repeated using the same grid size, but a much smaller dimensionless time step of 1×10^{-4}. The results obtained with the smaller time step confirmed what was found with the larger time step.

Similar results were also obtained when the coarser grid mesh of 31×91 was employed. Figure 6 shows time-sequence

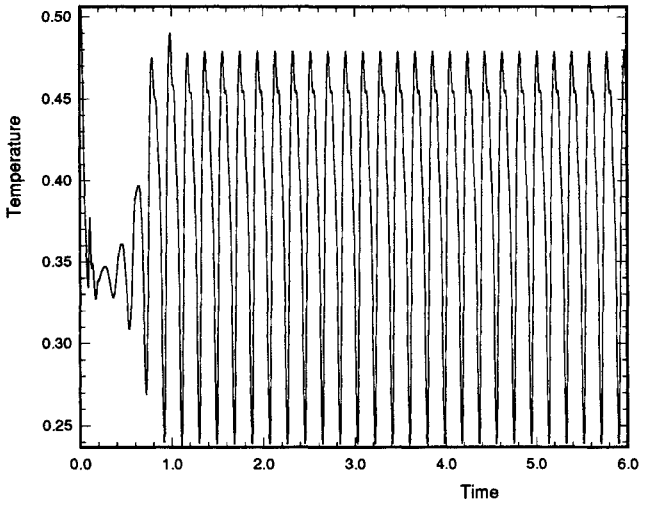

Fig. 5 Time evolution of temperature at $\zeta = 0.43$ for $\vartheta = -30$ deg, $Gr = 6.0 \times 10^4$; solution corresponding to $Gr = 2.0 \times 10^4$ specified as the initial condition, grid mesh 51×151, time step 5×10^{-4}.

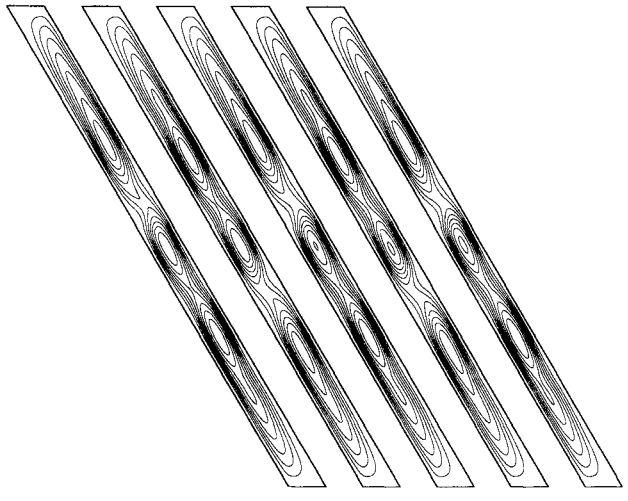

Fig. 6 Time sequence of stream function field; $\vartheta = -30$ deg, $Gr = 6.0 \times 10^4$ time interval 0.0935.

plots of the stream function field for this unsteady flow in dimensionless time intervals of 0.0935 for one period of oscillation. As illustrated by the time-sequence stream function plots, the unsteadiness in the flow corresponds primarily to an oscillation of the outer cell centers about the cavity center point. This numerical scheme predicts that the outer cells move apart or come closer together (relative to the center cell) in such a way that the centro-symmetry condition is not maintained. A similar flow structure was recently presented by Le Quere[14] for a vertical cavity of aspect ratio 16. Le Quere[14] attributed these oscillations to transient effects.

Lee and Korpela[9] indicated that the flow structure may also depend on the initial condition. As a result, an attempt was made to investigate the effect of the initial condition on the flow structure which is predicted by this numerical scheme. We have already seen that an unsteady flow structure is predicted at $Gr = 6.0 \times 10^4$ if the solution correponding to $Gr = 2.0 \times 10^4$ is specified as the initial condition. However, when zero was specified as the initial condition for $Gr = 6.0 \times 10^4$, then a steady-state solution was achieved at a dimensionless time approximately equal to 2, as shown in Fig. 7 by the time trace of the temperature at a point located along the vertical centerline and at $\zeta = 0.43$. These results are consistent with the results of Lee and Korpela[9] that the solution depends on the initial condition which is specified. Furthermore, these results suggest that, depending on the initial condition specified, steady as well as unsteady solutions may be obtained for some ranges of Gr values. The stream function-temperature plots (Fig. 3d and Fig. 4d) indicate that the flow corresponding to this solution branch is characterized by a two-cell structure which again breaks the centro-symmetry condition.

Starting from rest and increasing Gr to 8.0×10^4, the flow is now predicted to be monocellular and, in addition, steady, if a grid mesh of 31×91 or 51×151 is used. As shown in Fig. 4e, the temperature field corresponding to this Gr value is highly stratified in the center region, meaning that the temperature increases with height.

Figures 8 and 9 show results for the stream function and temperature field for an inclination angle of negative 15 deg. In this case, the transition to multicellular flow occurs at a lower Gr number than in the case when $\vartheta = -30$ deg. Once the hydrodynamic instability appears, the flow is described by a steady four-cell structure. The transition to the three-cell, two-cell, and monocellular structure occurs consistently at much lower Gr values at this inclination angle, as compared to the case when $\vartheta = 30$ deg. Based on the cases analyzed, a steady-state solution was achieved (with both grid sizes) at this inclination angle for all Gr values considered when the

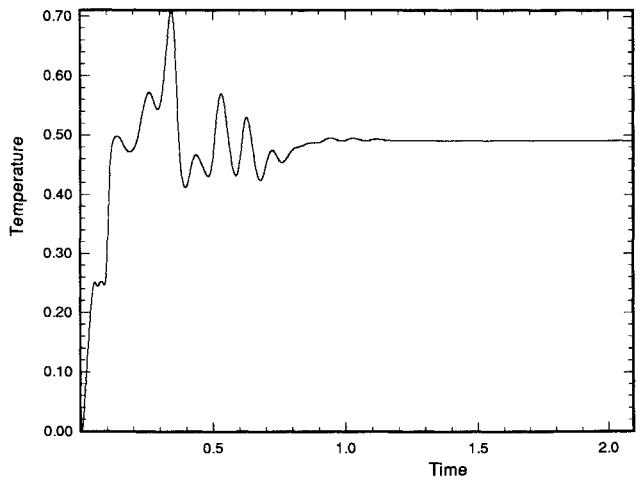

Fig. 7 Time evolution of temperature at $\zeta = 0.43$ for $\vartheta = -30$ deg, $Gr = 6.0 \times 10^4$ and zero specified as the initial condition; grid mesh 51×151, time step 5×10^{-4}.

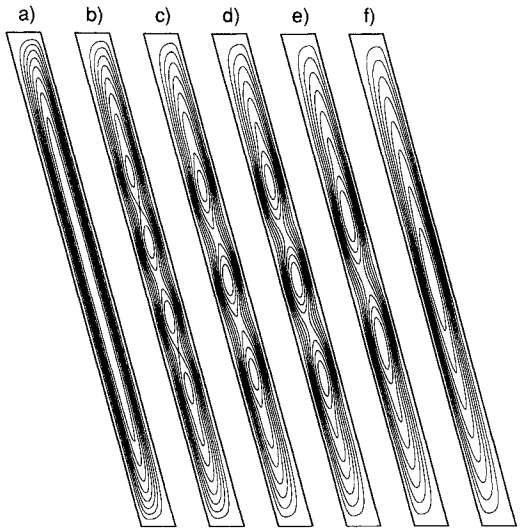

Fig. 8 Stream function contours for $\vartheta = -15$ deg: a) $Gr = 9.0 \times 10^3$, b) $Gr = 1.2 \times 10^4$, c) $Gr = 2.0 \times 10^4$, d) $Gr = 3.0 \times 10^4$, e) $Gr = 4.5 \times 10^4$, f) $Gr = 6.0 \times 10^4$.

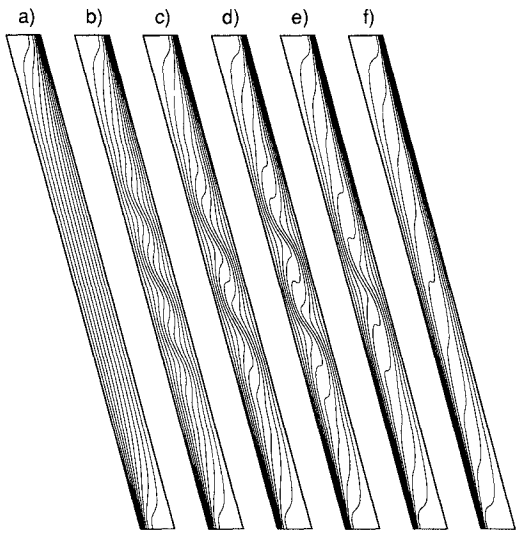

Fig. 9 Isotherms for $\vartheta = -15$ deg: a) $Gr = 9.0 \times 10^3$, b) $Gr = 1.2 \times 10^4$, c) $Gr = 2.0 \times 10^4$, d) $Gr = 3.0 \times 10^4$, e) $Gr = 4.5 \times 10^4$, f) $Gr = 6.0 \times 10^4$.

solution corresponding to the previous value of Gr was used as the initial condition.

Figures 10 and 11 show results for the stream function and temperature field for the special case of ϑ being equal to zero. The results presented here are in good agreement with the results of Korpela et al.,[8] Lee and Korpela,[9] and Ramanan and Korpela.[23] A steady-state solution was achieved (with both grid sizes) for all Gr values considered when the solution corresponding to the previous value of Gr was specified as the initial condition. Clearly, the flow undergoes a reverse transition from multicellular back to monocellular flow when Gr is approximately equal to 4.5×10^4.

As shown previously, the flowfield structure depends strongly on the initial condition. This point was also experienced, as it will be shown, with the vertical cavity case. For when zero was specified as the initial condition, a monocellular flow structure was predicted at a Gr value approximately equal to 3.75×10^4, which is slightly lower than the value that was obtained (4.5×10^4) when the sequential approach of specifying the initial condition was used. This set of computations suggests that this numerical scheme predicts a reverse transition from multicellular flow back to monocellular flow, regardless of the initial condition used. The value of Gr for

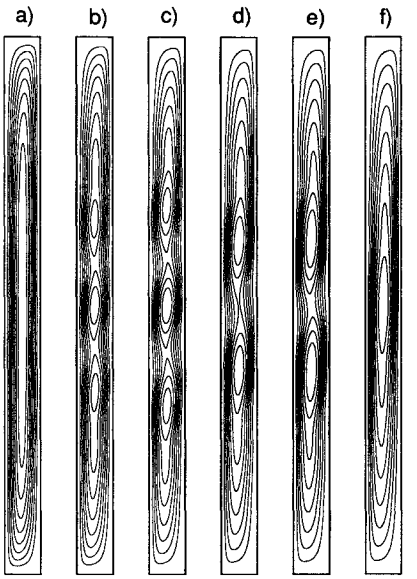

Fig. 10 Stream function contours for $\vartheta = 0$ deg: a) $Gr = 9.0 \times 10^3$, b) $Gr = 1.2 \times 10^4$, c) $Gr = 2.0 \times 10^4$, d) $Gr = 3.0 \times 10^4$, e) $Gr = 4.0 \times 10^4$, f) $Gr = 4.5 \times 10^4$.

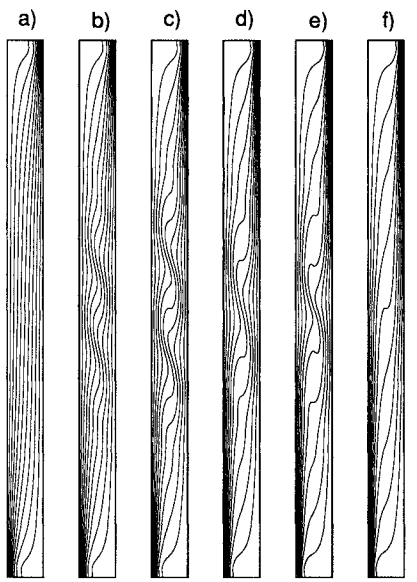

Fig. 11 Isotherms for $\vartheta = 0$ deg: a) $Gr = 9.0 \times 10^3$, b) $Gr = 1.2 \times 10^4$, c) $Gr = 2.0 \times 10^4$, d) $Gr = 3.0 \times 10^4$, e) $Gr = 4.0 \times 10^4$, f) $Gr = 4.5 \times 10^4$.

which this reverse transition occurs does, however, appear to vary with the initial condition.

The effects of heating from above on the flow structure are shown in Figs. 12 and 13 for an inclination angle of 15 deg. Comparing these results to those corresponding to $\vartheta = -15$ deg (Figs. 8 and 9), it is interesting to see that in this case the transition to multicellular flow occurs at a higher Gr value, whereas, the return to monocellular flow occurs at a lower Gr value.

Figures 14 and 15 show stream function and temperature field results obtained for an inclination angle of 30 deg. The transition to multicellular flow occurs at a much higher Gr than when $\vartheta = -30$ deg. Once again, steady-state solutions were achieved for all Gr values considered, using a grid of 31×91 and 51×151. It is interesting to see that the maximum number of cells in this case is three, as compared to five in the case of heating from below.

The variation of the local Nusselt number along the heated wall is shown in Fig. 16 for $Gr = 2.0 \times 10^4$ and for all angles

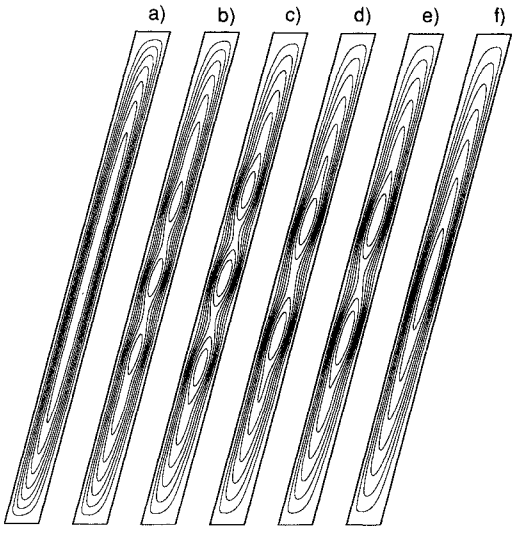

Fig. 12 Stream function contours for ϑ = 15 deg: a) Gr = 1.2 × 10^4, b) Gr = 1.5 × 10^4, c) Gr = 3.0 × 10^4, d) Gr = 3.5 × 10^4, e) Gr = 4.5 × 10^4, f) Gr = 6.0 × 10^4.

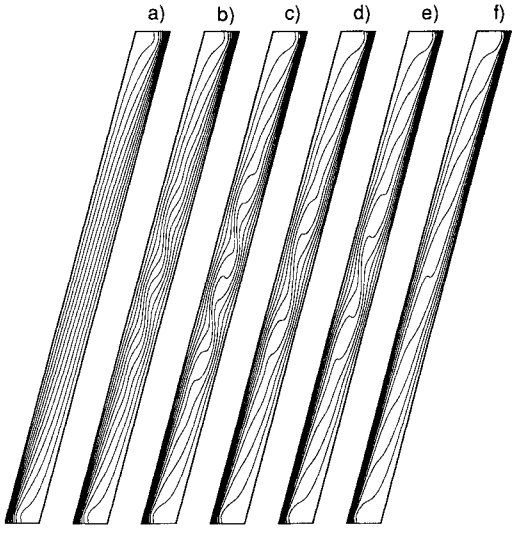

Fig. 13 Isotherms for ϑ = 15 deg: a) Gr = 1.2 × 10^4, b) Gr = 1.5 × 10^4, c) Gr = 3.0 × 10^4, d) Gr = 3.5 × 10^4, e) Gr = 4.5 × 10^4, f) Gr = 6.0 × 10^4.

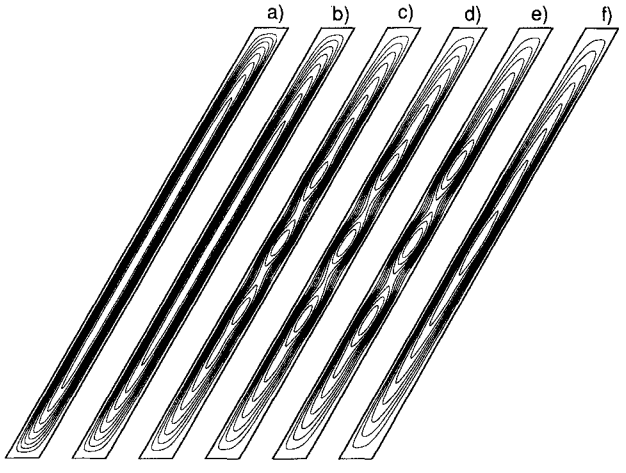

Fig. 14 Stream function contours for ϑ = 30 deg: a) Gr = 1.2 × 10^4, b) Gr = 2.0 × 10^4, c) Gr = 3.0 × 10^4, d) Gr = 4.5 × 10^4, e) Gr = 6.0 × 10^4, f) Gr = 8.0 × 10^{-4}.

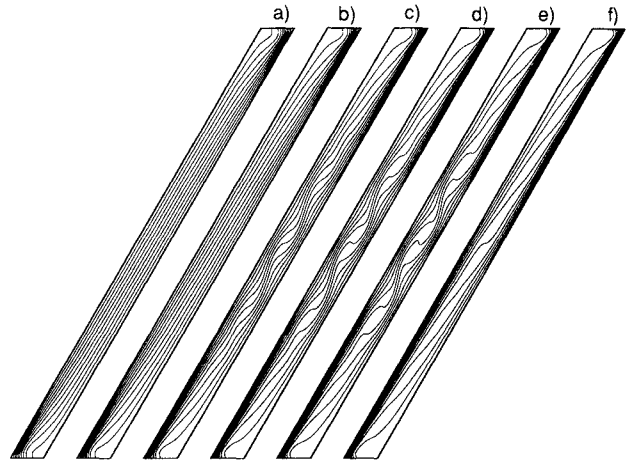

Fig. 15 Isotherms for ϑ = 30 deg: a) Gr = 1.2 × 10^4, b) Gr = 2.0 × 10^4, c) Gr = 3.0 × 10^4, d) Gr = 4.5 × 10^4, e) Gr = 6.0 × 10^4, f) Gr = 8.0 × 10^{-4}.

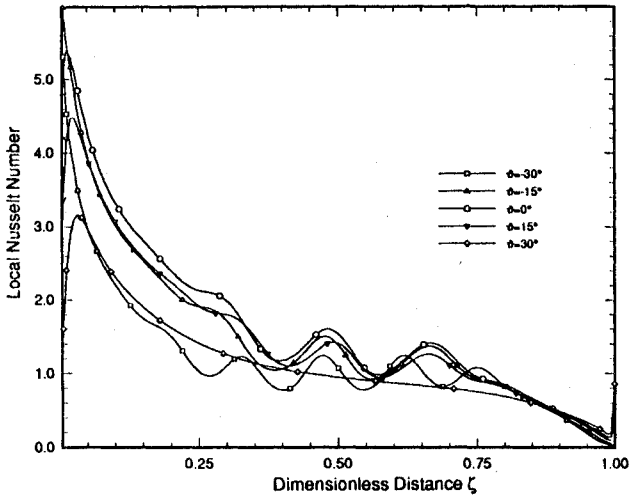

Fig. 16 Local Nusselt number distribution along heated wall, Gr = 2.0 × 10^4.

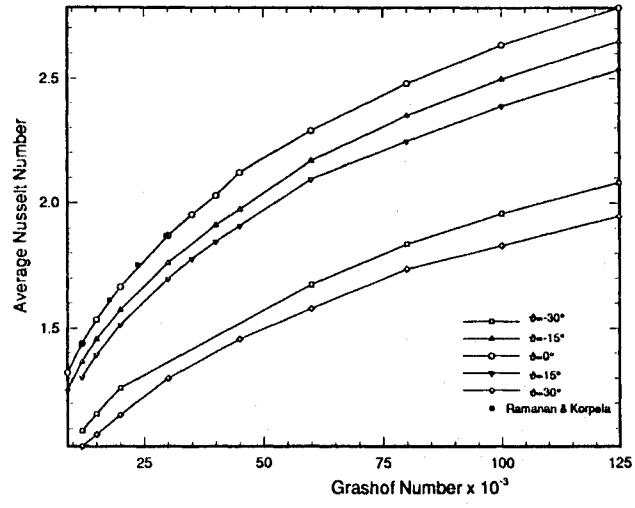

Fig. 17 Average Nusselt number vs Grashof number for different angles of inclination.

of inclination considered. As it can be seen, the presence of the transverse rolls in the center of the cavity cause large fluctuations on the local Nusselt number. It is important to note that Fig. 16 does not show the values for the local Nusselt number at ζ = 0.0 for ϑ = 30 deg and ϑ = 15 deg, which were calculated to be equal to 21.7 and 16.3, respectively.

Plots of the average Nusselt number as a function of ϑ and Gr are shown in Fig. 17 for all cases considered. Figure 17

shows that the results are in excellent agreement with the results (converted to the notation used by this study) obtained for a vertical cavity of aspect ratio 15 by Ramanan and Korpela[23] using a highly accurate multigrid solution technique. As expected, higher heat transfer rates result when the heating is from below.

Conclusion

Laminar free convection in a two-dimensional nonrectangular inclined cavity has been analyzed numerically. It is found that a multicellular flow structure is exhibited for all inclination angles considered. In addition, steady as well as unsteady flows were found for a range of *Gr* values. Although steady-state solutions were achieved for all Grashof numbers and angles of inclination considered, the flow structure (steady vs unsteady) was found to depend strongly on the initial condition and, in some cases, unsteady flows were predicted if the wrong initial condition was specified.

References

[1]Catton, I., "Natural Convection in Enclosures," *6th International Heat Transfer Conference*, Toronto, Canada, 1978, pp. 13–31.

[2]Ostrach, S., "Natural Convection in Enclosures," *Journal of Heat Transfer*, Vol. 110, 1988, pp. 1175–1190.

[3]Batchelor, G. K., "Heat Transfer by Free Convection Across a Closed Cavity Between Vertical Boundaries at Different Temperatures," *Quarterly Journal of Applied Mathematics*, Vol. 12, No. 3, 1954, pp. 209–233.

[4]Hart, J. E., "Stability of the Flow in a Differentially Heated Inclined Box," *Journal of Fluid Mechanics*, Vol. 47, Pt. 3, 1971, pp. 547–576.

[5]Korpela, S. A., Gozum, D., and Baxi, C. B., "On the Stability of the Conduction Regime of Natural Convection in a Vertical Slot," *International Journal of Heat and Mass Transfer*, Vol. 15, 1973, pp. 1683–1690.

[6]Elder, J. W., "Laminar Free Convection in a Vertical Slot," *Journal of Fluid Mechanics*, Vol. 23, Pt. 1, 1965, pp. 77–98.

[7]Vest, C. M., and Arpaci, V. S., "Stability of Natural Convection in a Vertical Slot," *Journal of Fluid Mechanics*, Vol. 36, 1969, pp. 1–15.

[8]Korpela, S. A., Lee, Y., and Drummond, J. E., "Heat Transfer Through a Double Pane Window," *Journal of Heat Transfer*, Vol. 104, Aug. 1982, pp. 539–544.

[9]Lee, Y., and Korpela, S. A., "Mulicellular Convection in a Vertical Slot," *Journal of Fluid Mechanics*, Vol. 126, Pt. 1, 1983, pp. 91–121.

[10]Schinkel, W. M. M., "Natural Convection in Inclined Air Filled Enclosures," Ph.D. Dissertation, Univ. of Technology, Delft, The Netherlands, 1980.

[11]Linthorst, S. J. M., Schinkel, W. M. M., and Hoogendoorn, C. J., "Flow Structure with Natural Convection in Inclined Air-Filled Enclosures," *Journal of Heat Transfer*, Vol. 103, Aug. 1981, pp. 535–539.

[12]Lauriat, G., and Desrayaud, G., "Natural Convection in Air-Filled Cavities of High Aspect Ratios: Discrepancies Between Experimental and Theoretical Results," American Society of Mechanical Engineers Paper 85-HT-37, Aug. 1985.

[13]Pignatel, J. F., and Marcillat, J. F., "Transition to Time-Dependent Free Convection in an Inclined Air Layer," *International Journal of Heat and Fluid Flow*, Vol. 7, No. 3, 1986, pp. 169–178.

[14]LeQuere, P., "A Note on Multiple and Unsteady Solutions in Two-Dimensional Convection in a Tall Cavity," *Journal of Heat Transfer*, Vol. 112, Nov. 1990, pp. 965–974.

[15]Roux, B., Grondin, J., Bontoux, P., and de Vahl Davis, G., "Reverse Transition from Multicellular to Monocellular Motion in a Vertical Fluid Layer," *Physico Chemical Hydrodynamics*, Vol. 3F, 1980, pp. 292–297.

[16]Gill, A. E., "The Boundary-layer Regime for Convection in a Rectangular Cavity," *Journal of Fluid Mechanics*, Vol. 26, Pt. 3, 1966, pp. 515–536.

[17]Ozoe, H., Sayama, H., and Churchill, S., "Natural Convection in a Inclined Rectangular Channel at Various Aspect Ratios and Angles—Experimental Measurements," *International Journal of Heat and Mass Transfer*, Vol. 18, 1975, pp. 1425–1431.

[18]Gray, D. D., and Giorgini, A., "The Validity of the Boussinesq Approximation for Liquids and Gases," *International Journal of Heat and Mass Transfer*, Vol. 19, 1976, pp. 545–551.

[19]Baron, A., "Flow Field and Heat Transfer Associated with a Forward Facing Step," Ph.D. Dissertation, Drexel Univ., Philadelphia, PA, 1987.

[20]Facas, G., and Mattioli, T., "Calculations of Two-Dimensional Laminar Flow in an Inclined Cavity Using a PC," *ASME Winter Annual Meeting*, HTD-Vol. 185, Atlanta, GA, 1991, pp. 55–60.

[21]Arakawa, A., "Computational Design for Long-Term Numerical Integration of the Equations of Fluid Motion: Two-Dimensional Incompressible Flow. Part I," *Journal of Computational Physics*, Vol. 1, 1966, pp. 119–143.

[22]Schneider, G. E., and Zedan, M., "A Modified Strongly Implicit Procedure for the Numerical Solution of Field Problems," *Numerical Heat Transfer*, Vol. 4, 1981, pp. 1–19.

[23]Ramanan, N., and Korpela, S. A., "Multigrid Solution for Natural Convection in a Vertical Slot," *Numerical Heat Transfer, Part A*, Vol. 15, 1989, pp. 323–339.